

MODELLING VEGETATION-ATMOSPHERE CO₂ EXCHANGE BY A COUPLED EULERIAN-LAGRANGIAN APPROACH

CHUN-TA LAI^{1,*}, GABRIEL KATUL¹, DAVID ELLSWORTH^{1,2} and RAM OREN¹

¹*School of the Environment, Box 90328, Duke University, Durham, NC 27708-0328, U.S.A.;*

²*Brookhaven National Laboratory, Upton, NY, U.S.A.*

(Received in final form 26 October 1999)

Abstract. A Eulerian-Lagrangian canopy microclimate model was developed with the aim of discerning physical from biophysical controls of CO₂ and H₂O fluxes. The model couples radiation attenuation with mass, energy, and momentum exchange at different canopy levels. A unique feature of the model is its ability to combine higher order Eulerian closure approaches that compute velocity statistics with Lagrangian scalar dispersion approaches within the canopy volume. Explicit accounting for within-canopy CO₂, H₂O, and heat storage is resolved by considering non-steadiness in mean scalar concentration and temperature. A seven-day experiment was conducted in August 1998 to investigate whether the proposed model can reproduce temporal evolution of scalar (CO₂, H₂O and heat) fluxes, sources and sinks, and concentration profiles within and above a uniform 15-year old pine forest. The model reproduced well the measured depth-averaged canopy surface temperature, and CO₂ concentration profiles within the canopy volume, CO₂ storage flux, net radiation above the canopy, and heat and mass fluxes above the canopy, as well as the velocity statistics near the canopy-atmosphere interface. Implications for scaling measured leaf-level biophysical functions to ecosystem scale are also discussed.

Keywords: Canopy turbulence, Lagrangian stochastic model, Turbulence closure, Canopy photosynthesis, Carbon dioxide, Radiation attenuation.

1. Introduction

Quantifying the exchange of matter, energy, and momentum between the biosphere and the atmosphere requires detailed understanding of the interactions between canopy structure and local canopy microclimate. The vertical structure of vegetation affects canopy microclimate by intercepting radiation, extracting momentum from the air flow aloft, and acting as a source or sink of mass and energy. In return, the microclimate surrounding vegetation directly impacts physiological and biophysical processes controlling carbon dioxide, heat, and water vapour exchange with the atmosphere. Over the past decade, many multi-level one-dimensional scalar transport models were developed to represent the complex interactions between the canopy microclimate and the atmosphere (Sawford, 1985; Meyers and Paw U, 1986, 1987; Raupach, 1988, 1989a; Baldocchi, 1992; Baldocchi et al., 1997; Baldocchi and Meyers, 1998). In describing scalar transport within the

* E-mail: C19@duke.edu



canopy, it was suggested by Raupach (1988, 1989a,b) that Lagrangian transport approaches are better suited than their Eulerian counterpart given their ability to overcome flux-gradient closure model limitations (Corrsin, 1974; Deardorff, 1978; Sreenivasan et al., 1982; Wilson, 1988). Such a conclusion resulted in a class of one-dimensional vegetation-atmosphere models (now known as *CANVEG*) that successfully combine physiological and biochemical functions derived from leaf-level measurements, radiation attenuation, and canopy microclimate to estimate scalar fluxes above the canopy (Baldocchi, 1992; Baldocchi et al., 1997; Baldocchi and Meyers, 1998).

In such models, velocity statistics, particularly vertical velocity standard deviation (σ_w) and Lagrangian integral time scales (T_L) within the canopy, must be assumed or specified a priori. Detailed velocity statistics such as σ_w are rarely measured within the canopy and cannot be readily specified for an arbitrary leaf area density distribution. Thus, current *CANVEG* models are unable to explicitly consider the role of canopy structure on momentum exchange, which is required to produce velocity statistics used in modelling scalar transport within the canopy volume.

Field experiments demonstrated that σ_w and T_L inside canopies are influenced by foliage distribution (Meyers and Paw U, 1986; Raupach, 1988, 1989a,b). These two flow variables provide the necessary inputs for Lagrangian mass transport calculations. One approach to account for the effects of foliage distribution on σ_w is higher-order Eulerian closure models. Higher-order closure models, developed over the past two decades (e.g., Wilson and Shaw, 1977; Lewellen et al., 1980; Shaw and Pereira, 1982; Meyers and Paw U, 1986; Wilson, 1988; Meyers and Baldocchi, 1991; Katul and Albertson, 1998; Massman and Weil, 1999), provide promising methodologies to link foliage distribution with such flow statistics.

Hence, we propose to circumvent such limitations by including a higher-order Eulerian closure approach to compute velocity statistics (particularly for σ_w) for use in Lagrangian scalar transport within the *CANVEG* framework. The combined Lagrangian-Eulerian approach is then used to estimate mean CO_2 concentration, sources and sinks distribution, and fluxes within the canopy. Model calculations are compared with measured scalar concentration profiles, remotely sensed skin temperature, and turbulent fluxes above a 15-year old uniform loblolly pine stand at the Duke Forest near Durham, North Carolina, U.S.A. Findings from this study will help guide future scaling efforts aimed at linking leaf level physiological and biophysical processes to canopy scale in a manner of conserving mass, momentum, energy, and radiation.

2. Theory

The basic conservation equations for scalar mass, radiation, energy, and momentum exchange within the canopy volume are considered next. Here, the canopy is di-

vided into layers, each of thickness dz , and all the equations below are employed at each layer.

2.1. SCALAR MASS BALANCE

For a horizontally uniform and rigid canopy, the one-dimensional scalar fluxes can be described (after proper time and horizontal averaging) by the scalar conservation equation,

$$\frac{\partial \bar{C}}{\partial t} + \frac{\partial F_c}{\partial z} = S_c, \quad (1)$$

where \bar{C} is the mean scalar concentration, F_c is the mean vertical flux of a scalar entity C (e.g., CO₂, H₂O and temperature), and S_c is the mean vegetation source (or sink) strength at time t and height z above the ground surface. All mean quantities are subject to both time and horizontal averaging as described by Raupach and Shaw (1982). For simplicity, we use an overbar only to indicate both time and horizontal averages. The scalar conservation equation has three unknowns (\bar{C} , F_c , S_c) requiring further formulations for at least two of them. In contrast to earlier *CANVEG* models, the unsteady component (i.e., $\partial \bar{C} / \partial t$) is retained to account for the storage flux within the canopy volume, which can be significant for CO₂ in tall vegetation (Wofsy et al., 1993; Hollinger et al., 1994; Fan et al., 1995; Grace et al., 1995; Baldocchi et al., 1997; Lee, 1998).

One approach to establish the needed equations is to consider the interdependency between $S_c(z)$ and $\bar{C}(z)$ via Lagrangian dispersion approaches. Raupach (1988) introduced a dispersion matrix (D_{ij}) that relates concentration difference between a given level \bar{C}_z and a reference level above canopy (\bar{C}_r) to the scalar source strength by

$$\bar{C}_z - \bar{C}_r = \sum_{j=1}^N S_{cj} D_{ij} \Delta z_j, \quad (2)$$

where i and j are the indices for height and source/sink strength location, respectively, Δz_j is the discrete layer thickness within the canopy, and N is the number of layers within the canopy volume. The D_{ij} matrix is calculated from the probability density function of fluid parcel trajectories, given by

$$x_{i+1} = x_i + u_i \Delta t \quad (3a)$$

$$z_{i+1} = z_i + w_i \Delta t, \quad (3b)$$

where x_i and z_i are longitudinal and vertical positions of the fluid parcel, respectively, u_i is the longitudinal fluid parcel velocity at time t_i , and w_i is the

vertical parcel velocity calculated by Thomson's (1987) random-walk algorithm for a Gaussian turbulent flow field. The random-walk algorithm for w_i is given by

$$w_{i+1} = w_i + \left[-\frac{w_i}{T_L} + \frac{1}{2} \left(1 + \frac{w_i^2}{\sigma_w^2} \right) \frac{\partial \sigma_w^2}{\partial z} \right] \Delta t + \left(\frac{2\sigma_w^2}{T_L} \Delta t \right)^{1/2} d\Omega, \quad (4)$$

where Δt is the time step increment and $d\Omega$ is a random increment with zero mean and unit variance. We also assume that the Lagrangian parcel velocity statistics converge to its Eulerian counterpart. Boundary conditions for calculating D_{ij} are described in Appendix A. With regards to the Gaussian vertical velocity approximation in (4), we note that Lagrangian models that consider inhomogeneity and non-Gaussian turbulence have been developed and tested (see Luhar and Britter, 1989; Sawford, 1993; Wilson and Sawford, 1996). According to Wilson and Sawford (1996), such models that consider non-Gaussian turbulence perform no better than those subjected to Gaussian assumptions (also see Baldocchi, 1997).

To compute D_{ij} , σ_w is needed at all levels within the canopy volume. Such statistics can be readily inferred from the higher-order closure models described in the following section.

2.2. VELOCITY STATISTICS (MOMENTUM CONSERVATION)

In this study, the second-order closure model, formulated by Wilson and Shaw (1977) is used to compute velocity statistics within the canopy. The effect of canopy structure on σ_w , and hence on D_{ij} , is explicitly treated. In this study, we used the assumed T_L suggested by Raupach (1988) but calculated σ_w by the Wilson and Shaw (1977) model to generate D_{ij} . The closure model computes vertical variation in mean horizontal velocity and its standard deviation, mean momentum flux, and lateral and vertical velocity standard deviations if the leaf area density and foliage drag coefficient are known. Details of the second-order closure model of Wilson and Shaw (1977) are presented in Appendix B.

2.3. PHYSIOLOGICAL FUNCTIONS

Combining (1) and (2) provides only two equations for the three unknowns (i.e., \bar{C} , F_c , S_c), requiring further formulation for at least one unknown. The third prognostic equation is derived from physiological controls, in which vegetation sources and sinks can be linked to canopy structure using

$$S_c(z) = -\rho_a a(z) \frac{\bar{C}(z) - \bar{C}_i(z)}{r_b(z) + r_s(z)}, \quad (5)$$

where ρ_a is the mean air density, $a(z)$ is the leaf area density, \bar{C}_i is the mean intercellular scalar concentration at z , $r_b(z)$ is the leaf boundary-layer resistance, and

$r_s(z)$ is the stomatal resistance. Equations (1), (2), and (5) permit a complete mathematical description of \bar{C} , F_c and S_c if \bar{C}_i , r_s , and r_b are known or parameterized. In the following we describe the models for these three variables.

The leaf boundary-layer resistance for molecular diffusion is based on flat plate theory (Schuepp, 1993; Baldocchi and Meyers, 1998), given by

$$r_b = \frac{l_d}{d_m \text{Sh}}, \quad (6)$$

where l_d is a characteristic leaf length scale, d_m is the molecular diffusivity of a scalar entity, and Sh is the Sherwood number, which can be determined from the mean longitudinal velocity inside the canopy. The second-order closure model of Wilson and Shaw (1977), described in Appendix B, provides the necessary flow statistics for estimating r_b .

Describing r_s is much more difficult than r_b since shortwave radiation, leaf temperature, water vapour and ambient CO₂ concentration, as well as other variables, must be simultaneously considered (Aphalo and Jarvis, 1991; Leuning, 1995; Mott and Parkhurst, 1991; Monteith, 1995; Oren et al., 1998; Pataki et al., 1998).

Collatz et al. (1991) proposed a set of physiological and biochemical equations that link r_s to leaf photosynthesis (A_n), atmospheric relative humidity (h_s) and CO₂ concentration at the leaf surface (CO_{2s}), given by

$$g_s = m \frac{a_n h_s}{\text{CO}_{2s}} + b, \quad (7)$$

where m and b are empirical parameters that vary with vegetation type, and g_s ($= r_s^{-1}$) is the stomatal conductance. The biochemical model for CO₂ assimilation is described in Farquhar et al. (1980) and Leuning (1995), and has been widely tested for different vegetation types (Collatz et al., 1991; Harley et al., 1985, 1992; Baldocchi and Meyers, 1998). Appendix C presents the basic equations of the Collatz et al. (1991) model and Table I summarizes all the coefficients used in its parameterization for this particular forest. Clearly, estimating g_s requires that CO₂, H₂O, and heat transport be simultaneously considered with absorbed radiation and surface temperature. Hence, (1), (2), and (5) must be simultaneously solved for CO₂ and H₂O concentration, and temperature.

2.4. ENERGY BALANCE

The energy budget is employed at the leaf surface for each level within the canopy to compute the mean leaf surface temperature as well as absorbed radiation needed for estimating g_s . Due to non-linearity in the leaf energy budget equation, the two-term binomial expansion and Penman's (1948) approximation are used to derive an approximate explicit form to solve for the leaf temperature, given by

$$T_s = T_a + (Q_{ab} - \lambda_v g_v D_v / p_a - \epsilon \sigma T_a^4) / (h_c + \lambda_v g_v \Delta / p_a + 4\epsilon \sigma T_a^3), \quad (8)$$

TABLE I

Characteristic canopy properties and kinetic constants used in the model to calculate radiative transmission and stomatal conductance. The clumping factor was estimated from Baldocchi and Meyers (1998) who reported clumping factors varying from 0.73 to 0.84 in forests.

Variables	Value	Units	Source
Leaf area index, a_l	2.93		Ellsworth (1999)
Characteristic leaf length, l_d	0.001	m	Ellsworth (1999)
Clumping factor, Π	0.8		Baldocchi and Meyers (1998)
Spherical leaf distribution, x_e	1.0		Campbell and Norman (1998)
V_m @ 25 °C	59	$\mu\text{mol m}^{-2} \text{s}^{-1}$	Ellsworth (1999)
Stomatal slope factor, m	5.9		Ellsworth (1999)
Stomatal intercept factor, b	0.015		Ellsworth (1999)
Quantum efficiency, e_m	0.08		Collatz et al. (1991)
Michaelis constant for CO ₂ , K_c	404	$\mu\text{mol mol}^{-1}$	De Pury and Farquhar (1997)
Inhibition constant for O ₂ , K_o	240	mmol mol^{-1}	De Pury and Farquhar (1997)
Leaf absorptivity for PAR, α_p	0.8		Campbell and Norman (1998)
CO ₂ /O ₂ specificity ratio, ω	2.6	$\text{mmol } \mu\text{mol}^{-1}$	Collatz et al. (1991)

where T_s and T_a are leaf and ambient air temperatures at height z , respectively, Q_{ab} is the absorbed radiation by the canopy, λ_v is the latent heat of vaporization, g_v is the water vapour conductance (derived from g_s and g_b for water vapour), D_v is the vapour pressure deficit, p_a is the atmospheric pressure, ϵ is the leaf emissivity, σ is the Stefan–Boltzmann constant, h_c is a convection coefficient, and Δ is the slope of saturation vapour pressure – temperature function. The linearization in (8) is reasonable if $|T_s - T_a| < 2$ °C.

2.5. RADIATION BALANCE

Radiative transfer throughout the canopy is critical to modelling Q_{ab} , and subsequently T_s . The incoming solar radiation was partitioned into longwave and shortwave radiation. For thermal or longwave radiation, the atmosphere was assumed to function as a grey body (Campbell and Norman, 1998). This allows the use of an averaged sky emissivity for calculating the atmospheric thermal emittance. We note that this assumption is crude because the uncertainty in the averaged sky emissivity is large, especially for cloudy conditions. The shortwave radiation was divided into direct beam radiation and diffuse radiation (Campbell and Norman, 1998). After reducing separately incident photosynthetically active radiation (PAR) and near-infrared radiation (NIR) by the radiation reflected from the canopy top, the remaining radiation is then transmitted through the canopy. Campbell and Norman's (1998) light transmission model is used to estimate the sunlit and shaded

portion of foliage at each canopy level and, consequently, estimate the radiation flux density absorbed by the foliage. The fraction $\tau_b(\psi)$ of incident beam radiation from a zenith angle ψ that penetrates through the canopy is given by

$$\tau_b(\psi) = \exp(-\sqrt{\alpha} K_{be}(\psi) a_l \Pi), \quad (9)$$

where α is the leaf radiation absorptivity, $K_{be}(\psi)$ is the extinction coefficient for ellipsoidal leaf distribution, $a_l (= \int_0^{z_h} a(z) dz$ where z_h is the canopy height) is the leaf area index, and Π is the clumping factor of leaf distribution. The absorptivity is defined with $\alpha = 1$ for a black body, and for canopy radiation transmission, the typical values are $\alpha = 0.8$ for PAR and $\alpha = 0.2$ for NIR.

For ellipsoidal leaf distribution, $K_{be}(\psi)$, defined by the fraction of leaf area projected onto a horizontal plane from a particular ψ , can be calculated by (Campbell and Norman, 1998)

$$K_{be}(\psi) = \frac{\sqrt{x_e^2 + \tan^2 \psi}}{x_e + 1.774(x_e + 1.182)^{-0.733}}, \quad (10)$$

where x_e is the ratio of average projected area of canopy elements on the horizontal and vertical surfaces (e.g., for a spherical leaf distribution, $x_e = 1$; for a vertical distribution, $x_e = 0$; and for a horizontal leaf canopy, x_e approaches infinity). Typically, $x_e = 1.0$ and $\Pi = 0.8$ for conifers.

2.6. TIME-DEPTH INTEGRATION

The required input variables in the model are 30-minute mean meteorological conditions at some reference height above the canopy (i.e., air temperature, water vapour and CO₂ concentrations, mean longitudinal velocity, and photosynthetically active radiation), and all radiative, physiological, biophysical, and drag properties of the canopy (i.e., $a(z)$, l_d , Π , α , and the kinetic constants listed in Table I). The model calculates mean concentration, sources, sinks and fluxes within and above the canopy for heat, CO₂ and H₂O. Additionally, intercellular CO₂ concentration, leaf surface temperature, absorbed radiation, and first-order and second-order flow statistics at all levels within the canopy are computed.

The lower boundary conditions for the flow are attributed to soil respiration and evaporation. We used the flow statistics from the Wilson and Shaw (1977) closure model and a gradient-diffusion approach that estimates the scalar ground fluxes $F_g(t)$ from the CO₂ and water vapour concentration gradients. We assumed a turbulent boundary-layer approximation in conjunction with Monin–Obukhov similarity theory at the forest-floor with fluxes determined from measured concentration near the ground ($z = 10$ cm). Hence, an integrated flux-gradient approach for the lower boundary conditions for CO₂, H₂O, and heat is adopted with the turbulent diffusivity near the forest floor computed from modelled σ_w and Reynolds stress $\overline{u'w'}$.

By considering the scalar storage within each canopy layer, the impact of unsteadiness in the scalar conservation equation is incorporated. The scalar storage flux $F_s(t)$ is calculated by integrating $\partial\bar{C}/\partial t$ between 0 and z_h , and is given by

$$F_s(t) = \int_0^{z_h} \frac{\partial\bar{C}}{\partial t} dz. \quad (11)$$

The model calculations are performed as follows:

- (i) Generate the turbulent velocity statistics using the assumed drag coefficient, measured $a(z)$, and the second-order closure model described in Appendix B.
- (ii) Using the modelled \bar{U} , σ_w from step (i) along with assumed T_L , compute D_{ij} using Thomson's random walk algorithm.
- (iii) For each 30-minute time step, Equations (1)–(10) as well as the equations in Appendix C are simultaneously solved by initially assuming well-mixed temperature, H₂O, and CO₂ concentration within the canopy, and iteratively refining the calculations until no change in T_s is noted at all levels in the canopy between two successive iterations. Check if the linearization in (8) is reasonable (i.e., $|T_s - T_a| < 2^\circ\text{C}$).
- (iv) Storage rate corrections are then applied to (1) between two successive 30-minute time steps in an iterative manner. The details of such calculations are discussed in Section 4.4.

3. Experiment

3.1. STUDY SITE

The data set was collected during 24–31 August 1998 at the Blackwood Division of the Duke Forest near Durham, North Carolina (36°2'N, 79°8'W, elevation = 163 m). The site is a uniformly planted loblolly pine (*Pinus taeda* L.) forest that extends 300–600 m in the east-west direction and 1000 m in the north-south direction. The mean canopy height was 14.0 m (± 0.5 m) at the time of the experiment. The topographic variations are small (terrain slope changes $< 5\%$) so that the influence of topography on the turbulence transport can be neglected (Kaimal and Finnigan, 1994).

3.2. EDDY COVARIANCE MEASUREMENTS

The CO₂ and water vapour fluxes above the canopy were measured by an eddy-covariance system comprising of a Licor-6262 CO₂/H₂O infrared gas analyzer (LI-COR, Lincoln, NE, U.S.A.) and a Campbell Scientific triaxial sonic anemometer (CSAT3, Campbell Scientific, Logan, UT, U.S.A.). Figure 1 shows the experimental setup and the instrument heights relative to the canopy. The CSAT3

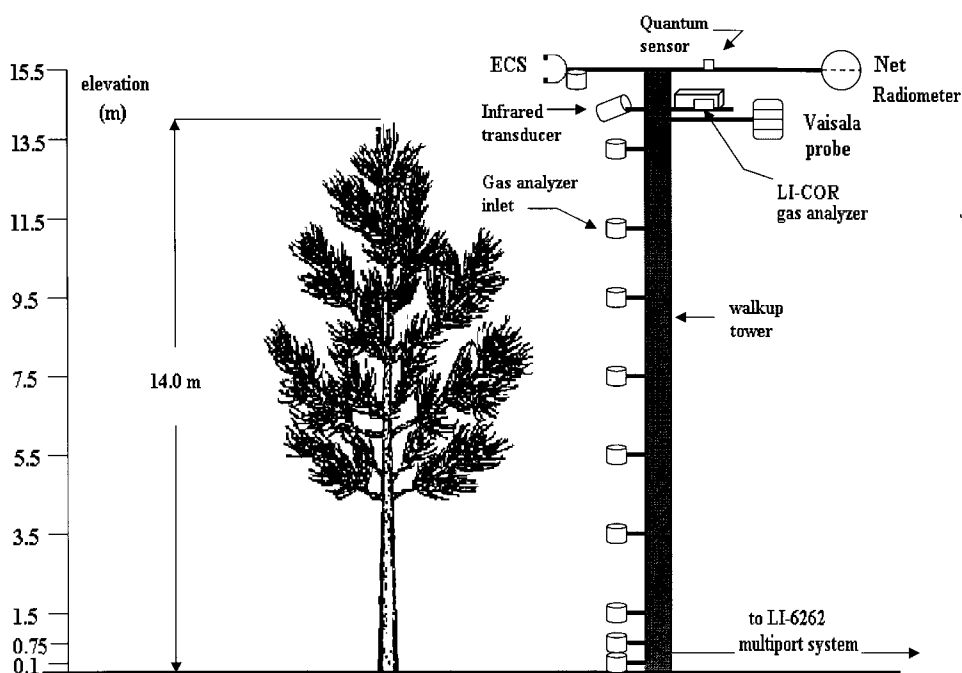


Figure 1. Schematic display of instrumentation heights for the experimental setup, where ECS represents the eddy-covariance system.

was positioned at 15.5 m above the ground surface, and was anchored on a horizontal bar extending 1.5 m away from the walkup tower. The infrared gas analyzer was housed in an enclosure 4.5 m from the inlet cup, which is positioned under the eddy covariance system. The sampling flow rate for the gas analyzer is 9 L min^{-1} , sufficient enough to maintain turbulent flow in the tubing. A krypton hygrometer (KH_2O , Campbell Scientific) was positioned with the CSAT3 to assess the magnitude of the tube attenuation and time lag between vertical velocity and scalar concentration fluctuations as discussed in Katul et al. (1997a,b).

The analog signals from these instruments were sampled at 10 Hz using a Campbell Scientific 21X data logger with all digitized signals transferred to a portable computer via an optically isolated RS232 interface for future processing. All 10 Hz raw measurements processing was performed using the procedures described in Katul et al. (1997a,b) with scalar covariance computed after maximizing the cross correlation between vertical velocity fluctuations and scalar concentration fluctuations for each 30 minute run. Other measurement and processing corrections are described in Katul et al. (1997a,b).

3.3. OTHER METEOROLOGICAL VARIABLES

In addition to the eddy covariance flux measurements above the canopy, a HMP32C Ta/RH (Vaisala) probe (Campbell Scientific) was positioned at the same height to measure the mean air temperature and relative humidity. A Q7 Fritchen type net radiometer and a LI-190SA quantum sensor (LI-COR) were installed to measure net radiation (R_n) and PAR, respectively. The net radiation measurements were also used to assess the energy closure. Using eddy-covariance measured latent and sensible heat fluxes and estimates of the heat storage flux within the canopy volume and soil heat flux (assumed at 10% of R_n), the closure was, on average, 90%. The mean skin temperature was measured using an infrared transducer (Everest Interscience, CA, U.S.A.) placed at 15 m and angled at 45°. The emissivity was set to 0.98 and was determined from runs in which sensible heat flux did not exceed 20 W m⁻² and friction velocity was greater than 0.5 m s⁻¹. All the meteorological variables were sampled at 1 s and averaged every 30 minutes using a 21X Campbell Scientific datalogger.

3.4. CO₂/H₂O PROFILES WITHIN THE CANOPY

A multi-port system was installed to measure the CO₂/H₂O concentrations inside the canopy at 10 levels (0.1 m, 0.75 m, 1.5 m, 3.5 m, 5.5 m, 7.5 m, 9.5 m, 11.5 m, 13.5 m and 15.5 m). Each level was sampled for one minute (45 s sampling and 15 s purging) at the beginning, the middle, and the end of a 30-minute sampling duration. The flow rate within the tube (internal diameter = 4 mm) was 0.9 L min⁻¹ to dampen all turbulent fluctuations.

3.5. LEAF-LEVEL PLANT PHYSIOLOGICAL PARAMETERS

The leaf-level measurements presented in Table I are described in Ellsworth (1999). The leaf-level physiological parameters (m and b) were determined from measurements by a portable infra-red gas analyzer system for CO₂ and H₂O (CIRAS-1, PP-Systems) operated in open flow mode with a 5.5-cm long leaf chamber and an integrated gas CO₂ supply system. The chamber was modified with an attached Peltier cooling system to maintain chamber temperature near ambient atmospheric temperature. The data were collected for upper canopy foliage at 11–12 m height, accessed with a system of towers and mobile vertically telescoping lifts. All measured gas exchange rates are reported on a unit projected area basis in this paper. For cylindrical pine needles, the projected area is obtained from the surface area A_s as $A_s/2.364$. These measurements were collected over a broad range of environmental conditions spanning a period of 1.5 years (May 1997–October 1998).

The mean soil moisture content (θ) in the root zone (0–30 cm) was 0.16 and was determined by averaging 24 CS 615 water content reflectometer rods (Campbell Scientific) over the entire experiment duration. Oren et al. (1998) demonstrated that soil moisture content exerts minor control on canopy stomatal conductance in

this stand for $\bar{\theta} > 0.2$. However, for $\bar{\theta} \cong 0.15$, the canopy stomatal conductance is diminished by 30% when compared to its value for $\bar{\theta} > 0.2$ under similar mean meteorological conditions. Hence, it is clear that the present experimental conditions, with $\bar{\theta} = 0.16$, cannot be classified as well watered. We note that the performance of the Collatz et al. model, described in Appendix C, is substantially reduced for dry soil moisture conditions (i.e., when g_s is primarily controlled by $\bar{\theta}$) (Baldocchi and Meyers, 1998). However, its performance for intermediate soil moisture content remains the subject of on-going investigation.

4. Results and Discussions

The ability of the model to reproduce measured scalar fluxes, mean scalar concentration profiles, and other characteristics of the canopy microclimate are investigated. In all calculations, the canopy is divided into one-metre planar homogeneous layers, and Equations (1)–(10) along with all equations in Appendices B and C are applied to each individual layer to solve for mean scalar concentration, sources and sinks, and vertical fluxes. For clarity, the velocity statistics used to drive much of the scalar transport calculations, and the radiation attenuation used to drive much of the modelled physiological sources and sinks, are considered first.

4.1. VELOCITY FIELD

Contrary to earlier Lagrangian dispersion model calculations, the present approach computes the flow field statistics based on the drag properties and leaf area distribution of the canopy. The second-order closure model of Wilson and Shaw (1977) was previously tested at a different location but in the same stand using a six-level velocity statistics profile experiment (Katul and Chang, 1999).

To further investigate the differences among the measured σ_w , the σ_w profiles generated by the Wilson and Shaw (1977) closure model and that suggested by Raupach (1988) at this particular location, we carried out a multi-level experiment to measure the flow statistics within the canopy at eight levels. The experimental setup and the results are shown in Appendix B. From the comparisons in Appendix B, the modelled σ_w was in good agreement with the measurements, while differences between Raupach's assumed profile and the measured σ_w is significant in the lowest layers of the canopy. Differences in σ_w gradients within such layers are critical to the D_{ij} calculations as evidenced from (4), particularly when σ_w is small. Hence, we performed a sensitivity analysis on D_{ij} using the modelled and Raupach's σ_w profiles and found a 65% difference in dispersion matrix values (see regression slopes in Table II). Figure 2 contrasts the two D_{ij} derived from the different σ_w profiles as shown in the Appendix B. Two groups of points emerged: the plus sign indicates the parcel concentrations at $z = 1$ m in the concentration profile, contributed by each unit source released from $z = 1$ to 14 m, while the open

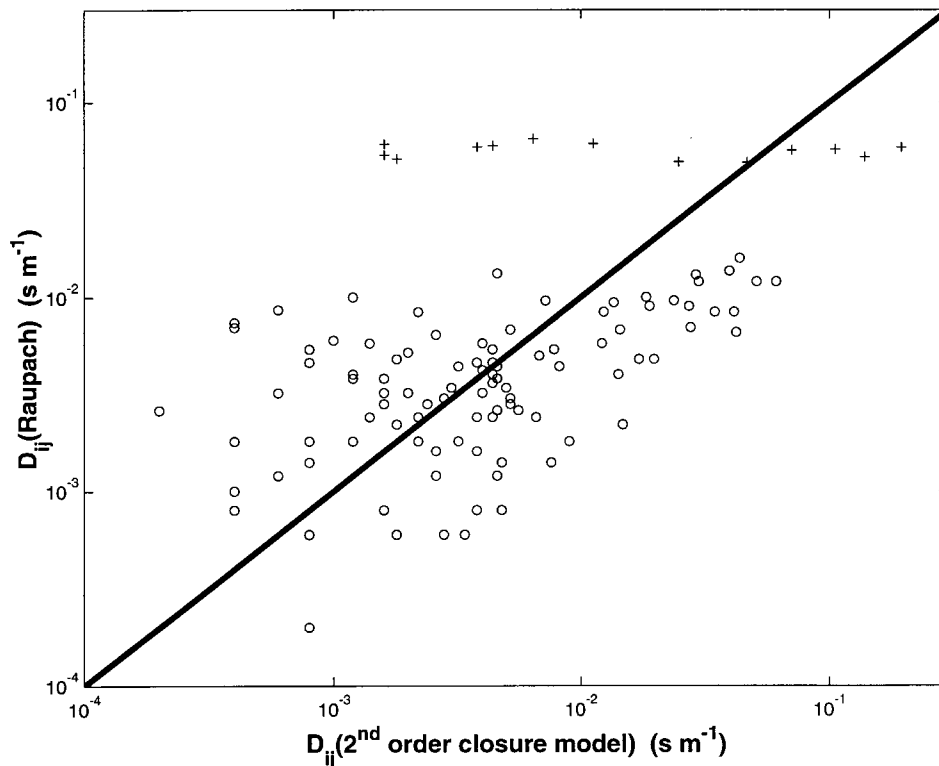


Figure 2. Comparison (open circles) between dispersion matrices (D_{ij}) computed from the σ_w profile suggested by Raupach (1988) with those computed after Wilson and Shaw (1977); i and j are concentration and unit source location indices, respectively. For clarity, the D_{1j} comparisons are shown in plus. The 1 : 1 line (solid) is also shown.

circles are for the remaining points. Using the suggested σ_w of Raupach (1988), the unit source at each z_j contributes about the same to \bar{C}_z at $z = 1$ m. However, using the velocity statistics generated by the second-order closure model, the contribution of each unit source to \bar{C}_z at $z = 1$ m diminishes with increasing height. The high D_{ij} values produced close to the ground by the closure-model calculations implies greater resistance to disperse the scalar concentration at that height, resulting in a higher concentration difference between ground level and the reference height, as described in (2). A quantitative comparison between the two computed D_{ij} is shown in Table II, suggesting great sensitivity to the specification of flow statistics. If the points for \bar{C}_z at $z = 1$ m (points designated at plus sign in Figure 2) are excluded from the D_{ij} comparison, the coefficient of determination (R^2) improves only slightly (see Table II). Hence, the contrast between the two D_{ij} calculations is not limited to a near-ground description of σ_w .

TABLE II

Model performance via comparisons between measured and modelled variables. The regression slope (A), the intercept (B), the coefficient of determination (R^2), and the standard error of estimate (SEE) are presented for the regression model $y = Ax + B$, where y and x are measured and modelled flow variables. Here, T_s is the skin temperature, LE is the latent heat flux, H is the sensible heat flux, \bar{C}_a is the mean CO₂ concentration inside the canopy and F_s is the storage flux. The i and j represent concentration and unit source location indices, respectively, and N is the number of points in the regression analysis. For the D_{ij} comparison, x is the D_{ij} computed from the Raupach (1988) velocity statistics.

Variable	Measurement/model type	N	A	B	R^2	SEE
D_{ij} (s m ⁻¹)	For $i = 1-15$ m; $j = 1-14$ m	210	0.35	0.004	0.27	0.012
D_{ij} (s m ⁻¹)	For $i = 2-15$ m; $j = 1-14$ m	196	0.20	0.02	0.33	0.003
T_s , (all data) (°C)	Infrared thermometer	322	1.02	-2.04	0.97	0.783
T_s , (day time) (°C)	Infrared thermometer	121	1.03	0.90	0.97	0.83
LE (W m ⁻²)	Eddy covariance at $z/z_h = 1.1$	322	0.85	-0.75	0.63	36.46
H (W m ⁻²)	Eddy covariance at $z/z_h = 1.1$	322	0.65	42.34	0.84	33.80
F_s (μmol m ⁻² s ⁻¹)	Gas analyzer at 10 levels	322	0.81	-0.01	0.57	2.42
F_c , (no storage) (μmol m ⁻² s ⁻¹)	Eddy covariance at $z/z_h = 1.1$	322	1.03	-2.52	0.52	4.19
F_c , (Scheme 1) (μmol m ⁻² s ⁻¹)	Eddy covariance at $z/z_h = 1.1$	322	0.62	-2.27	0.30	5.07
F_c , (Scheme 2) (μmol m ⁻² s ⁻¹)	Eddy covariance at $z/z_h = 1.1$	322	0.67	-2.29	0.35	4.89
\bar{C}_a , (no storage) (ppm)	Gas analyzer at 10 levels	2254	1.09	-35.14	0.84	19.54
\bar{C}_a , (Scheme 1) (ppm)	Gas analyzer at 10 levels	2254	1.09	-35.14	0.84	19.54
\bar{C}_a , (Scheme 2) (ppm)	Gas analyzer at 10 levels	2254	0.94	23.53	0.70	26.82

4.2. RADIATION TRANSFER

Much of the physiological sources and sinks are driven by absorbed radiation at different levels within the canopy. The radiation flux density absorbed by the leaves at each discrete layer is calculated separately for the sunlit and sun shaded fractions. To qualitatively illustrate the combined effects of sun angle, leaf area density distribution, canopy radiation transmission parameters and clumping, as well as cloud cover, on canopy radiation attenuation, the time-depth dynamics of the absorbed energy is displayed in Figure 3a. Notice in Figure 3a that much of the incoming energy is absorbed in the top 50% of the canopy. The absorbed radiation by the whole canopy can be calculated by integrating along z_h longwave and shortwave radiation absorbed at each discrete layer. In Figure 3b, a comparison

between the modelled absorbed radiation by the canopy and measured net radiation above the canopy is shown for the experimental duration. Differences between measurements and model calculations are due to the finite amount of energy flux density incident at the soil surface. This incident energy is dissipated as ground evaporation, sensible heat, and soil heat fluxes. These computed ground fluxes are used to drive the lower boundary conditions for heat and water vapour transfer.

While explicit evaluation of the radiation attenuation model was not performed, other indirect indicators can be used for validation. For example, modelled and measured mean leaf surface temperatures in the top 50% of the canopy are compared in Figure 3c. In this comparison, the modelled T_s is averaged for the top 50% for consistency with the calculated footprint of the measured infrared T_s . The model tends to systematically underestimate the measured surface temperature by 2 °C. Such underestimation can be attributed to many measurement and modelling factors, including the use of constant emissivity and fixed volume averaging for measured T_s , and the use of literature values for the canopy radiative properties (see Table I) without any modification. In addition, the footprint of the infrared transducer is an integral volume of leaves and branches resulting in higher mean T_s when compared to leaf temperature measurements only (Ewers and Oren, 1999).

Despite such a bias, the agreement between modelled and measured skin temperature was reasonable as evidenced by the regression statistics in Table II. The regression slope is 1.02 and $R^2 = 0.97$, with an intercept = -2.04 °C. The differences between modelled and measured T_s are more obvious during cloudy days (days 2 and 3) and evening runs (see Figure 3c). If we exclude these data points, the intercept reduces to +0.9 °C. These systematic offsets indirectly alter the modelled sensible heat fluxes shown in the next section.

4.3. SCALAR SOURCES, SINKS, FLUXES, AND CONCENTRATION WITHIN AND ABOVE THE CANOPY

The modelled source/sink strength for (a) CO₂, (b) H₂O and (c) heat is shown in Figure 4. Our calculations suggest clear dissimilarity between heat and the two other scalars in the source/sink strength distribution. While mid-day maximum CO₂ sinks and water vapour sources are co-located with maximum leaf area density, the maximum heat source strength is limited to within the top 25% of the canopy. This is attributed, in part, to the role of stomatal control on scalar but not heat transport. Much of the mechanisms that reduce the aerodynamic resistance, such as large wind speeds and radiation absorption, occur in the upper canopy layers despite the low leaf area density. While explicit assessment of the source strength and distribution calculation is not possible by direct field measurements, we consider two indirect validations: (1) comparisons between computed and measured scalar fluxes above the canopy, and (2) comparisons between modelled and measured scalar concentration within the canopy.

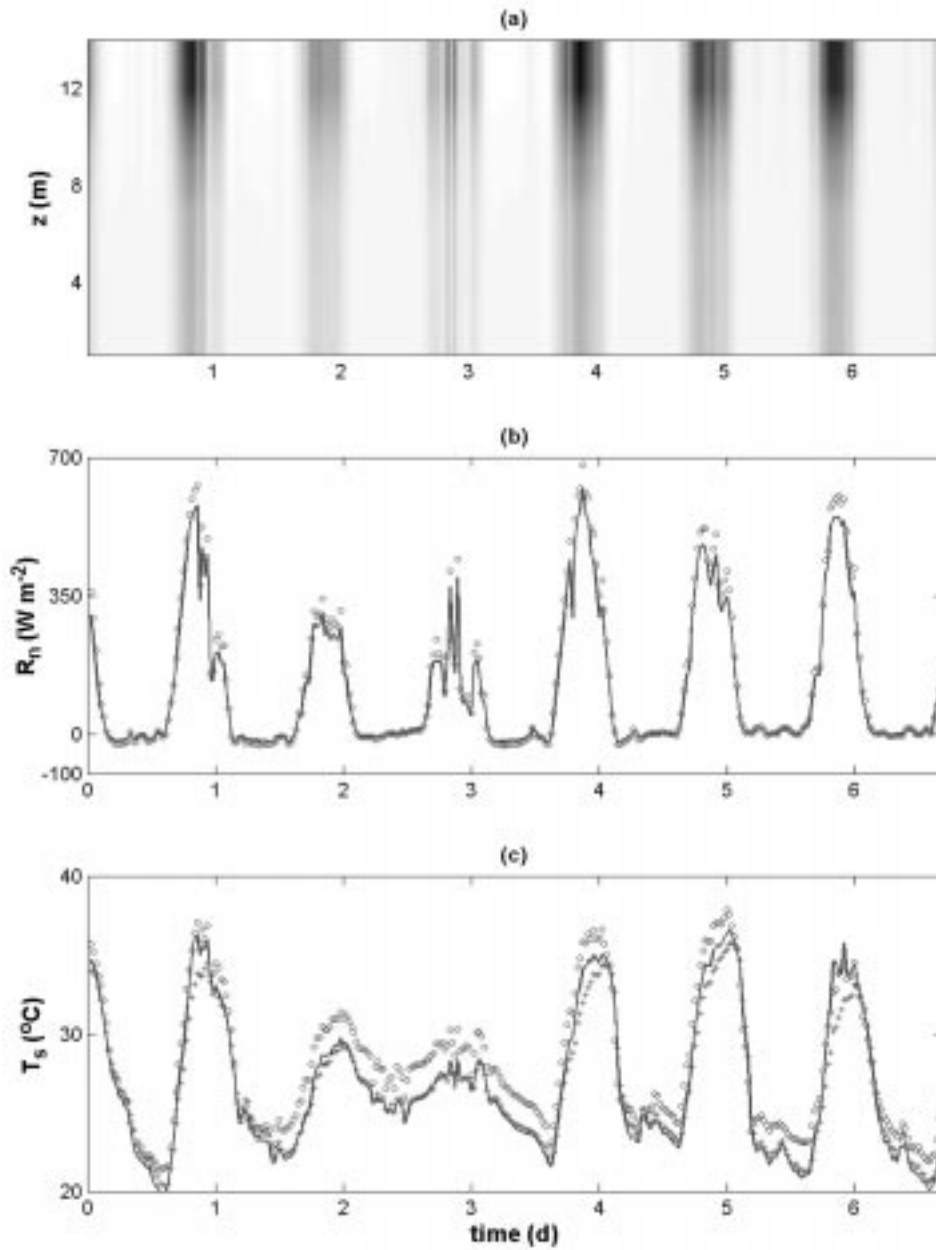


Figure 3. (a) Time-depth evolution of absorbed radiation by the canopy. Regions of maximum radiation absorption are in dark. (b) Comparison between modelled radiation absorbed by canopy (solid line) and net radiation measured above canopy (open circle). The difference is the incident radiation at the ground. (c) Comparison between measured (open circle) and modelled (solid line) depth-averaged ($z/z_h = [0.5 - 1]$) skin temperature. For reference, T_a (plus) is also shown.

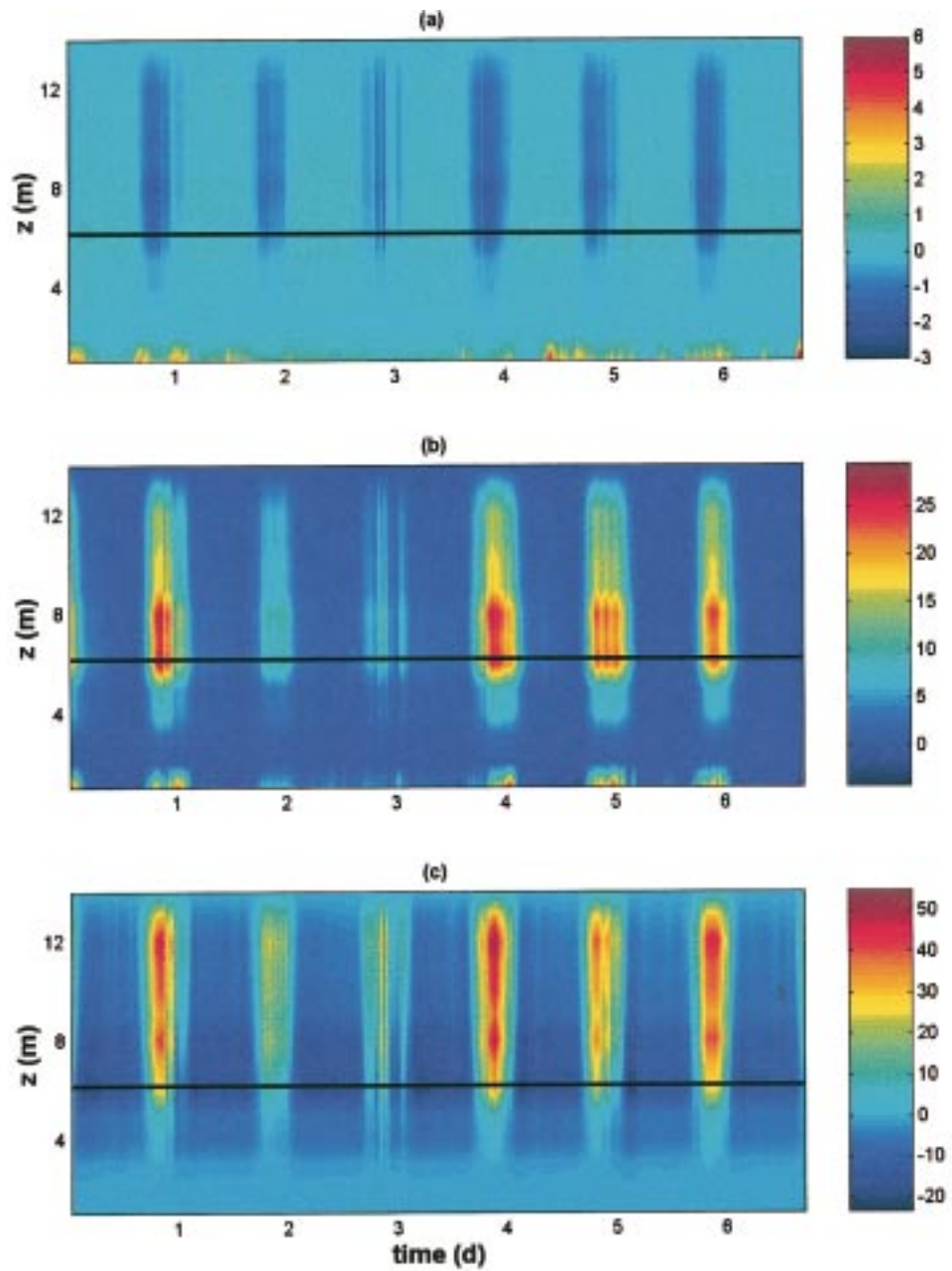


Figure 4. (a) Time-depth evolution of modelled source/sink strength for CO₂ ($\mu\text{mol m}^{-3} \text{s}^{-1}$). (b) Latent heat (W m^{-3}) and (c) sensible heat (W m^{-3}). The solid line indicates the height of maximum $a(z)$.

Reasonable agreements, between the modelled and measured diurnal patterns of CO₂, latent and sensible heat fluxes are noted in Figures 5(a), (b) and (c), respectively (see R² in Table II). From Table II (see slopes), the model appears to overestimate the measured H₂O flux above the canopy by 15%. While not significantly large when compared to the measurement uncertainty (Katul et al., 1999), such overestimation can be attributed to the fact that, (1) the parameters of the g_s model were derived from leaf level measurements (see Table I) that may not reflect all the leaves sensed by the eddy-covariance system, and (2) the hydrologic conditions (i.e., $\bar{\theta} < 0.2$) are less than optimal for the application of the Collatz et al. (1991) physiological model. In fact, the tendency of the model to overestimate the latent heat flux is consistent with previous assessments of the Collatz et al. model for dry conditions (Baldocchi and Meyers, 1998). Additionally, our model tends to underestimate the sensible heat flux during evening runs. Here, the model discrepancy with measurements is for nighttime runs and is due to the systematic biases in computed T_s as shown in Figure 3c.

To further investigate the adequacy of computed sources and sinks, Figure 6 shows the time-depth comparison between modelled and measured CO₂ concentration profiles inside the canopy volume. The model reproduced much of the dynamics in the measured concentration profiles despite a tendency to underestimate some events (see slopes in Table II). The systematic underestimation is primarily due to the crude parameterization of the soil CO₂ efflux, and the exclusion of atmospheric stability corrections inside the canopy. The effect of storage flux on CO₂ fluxes estimated above the canopy, and estimated CO₂ concentration within the canopy volume, is considered next.

4.4. STORAGE CALCULATION

The procedure to incorporate a storage term in (2) is not clear and may be approximate at best. This uncertainty is due to the fact that (2) applies for steady-state conditions while (1) can include transients in mean concentration. We investigated two different schemes to compute the storage flux. For reference, the results are contrasted to the negligible storage scenario in which $\partial\bar{C}/\partial t = 0$ in (1). These calculations are performed by first assuming steady-state conditions in (1) and (2) and determining \bar{C} for two consecutive 30-minute time steps. After estimating \bar{C} for each of the two successive 30-minute intervals, the following methods are considered:

1. Use these computed profiles to estimate $\partial\bar{C}/\partial t$ and re-calculate the scalar fluxes from (1). In this method, the relationship in (2) is unaffected by $\partial\bar{C}/\partial t$.
2. Represent $\partial\bar{C}/\partial t$ as a virtual source/sink term superimposed on the vegetation sources/sinks in (2) and redo all the calculations, including $\partial\bar{C}/\partial t$ corrections in (1), until the turbulent fluxes above the canopy do not change by more than 1% between two successive iterations.

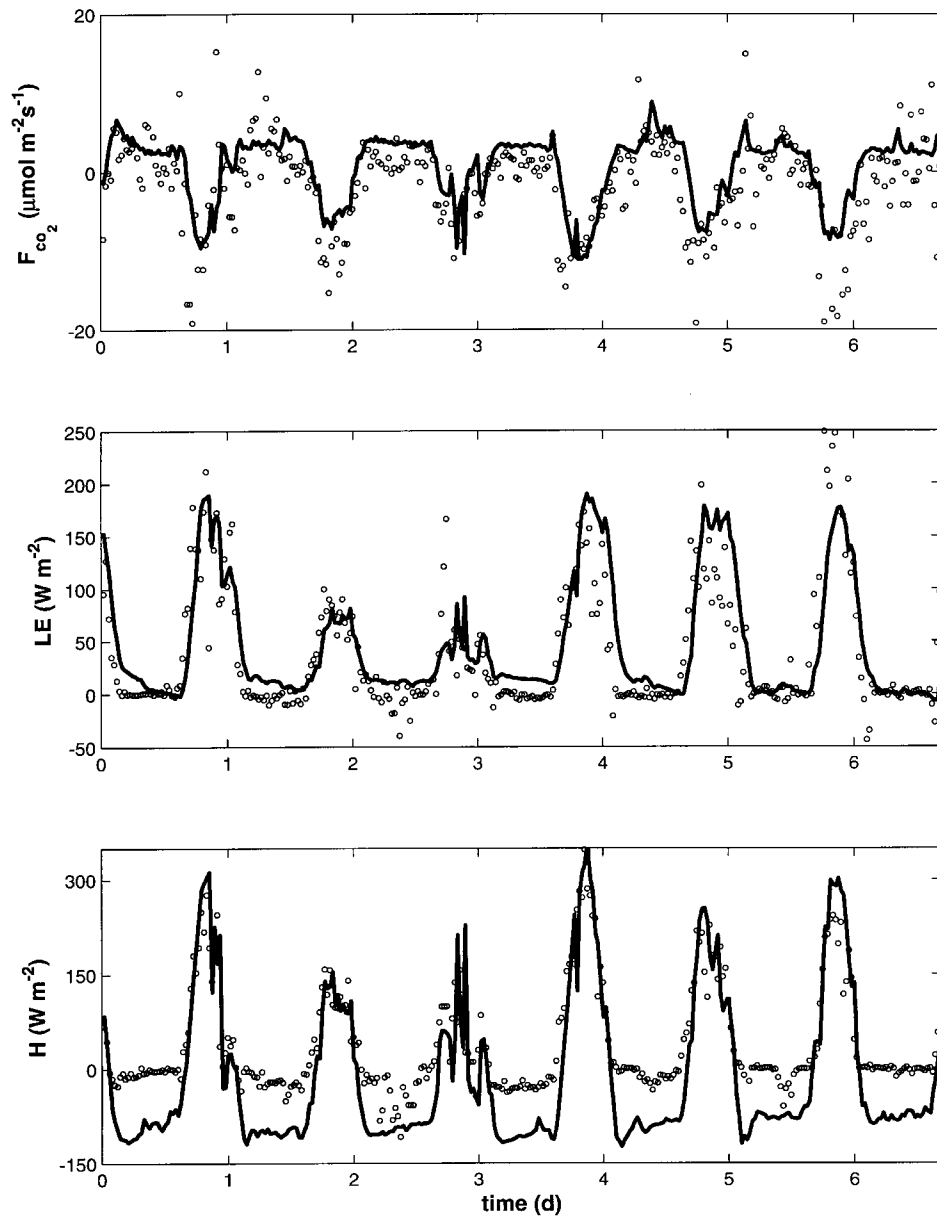


Figure 5. Comparisons between measured (open circle) and modelled (solid line) scalar fluxes (a) CO_2 , (b) latent heat (LE) and (c) sensible heat (H) fluxes above the canopy. The storage flux is not taken into account.

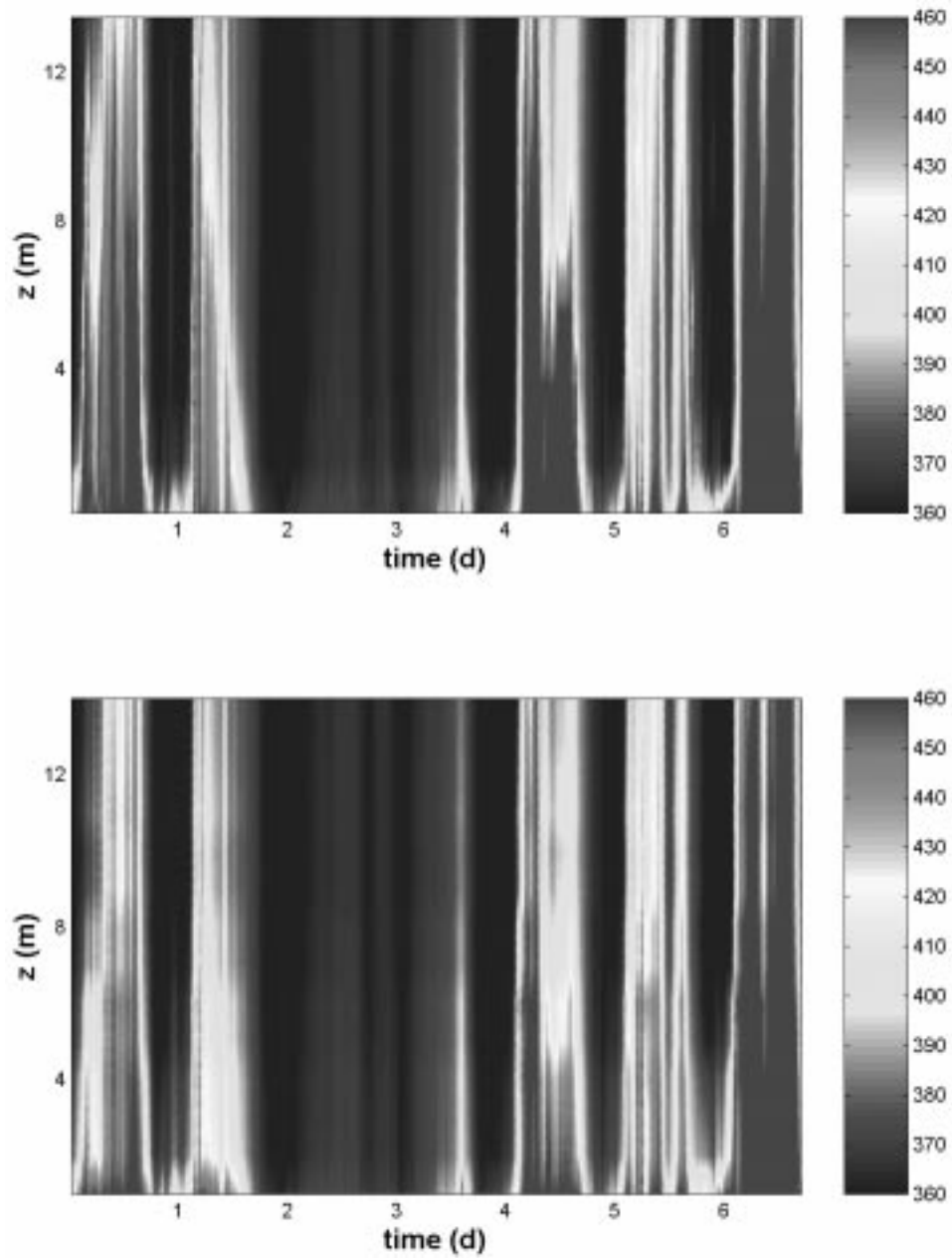


Figure 6. Time-depth evolution of measured (top) and modelled (bottom) CO₂ concentration ($\mu\text{mol mol}^{-1}$) inside the canopy.

We compared integrated storage (F_s) calculations with measurements in Figure 7a and found reasonable agreement between model and measurements for both methods (see Table II). The F_s is quite variable in time as evidenced in Figure 7a. Both modelled and measured F_s are substantially diminished for the two cloudy days when compared to non-cloudy days.

The CO_2 fluxes above the canopy, computed by accounting for the storage term via these two schemes are compared with the measured fluxes in Table II. From Table II, accounting for the storage flux term does not significantly improve the modelled flux or CO_2 concentration within the canopy (see regression statistics in Table II). Hence, while the model can reproduce the measured integrated storage flux as shown in Figure 7a, the fluxes above the canopy are predominantly governed by vegetation source/sink strength except for certain periods of the day (see Figure 7b). The results in Figure 7b are ensemble averaged by time of day using the modelled results in Figure 7a along with the modelled CO_2 fluxes above the canopy. The time in which F_s is important when compared to the CO_2 fluxes above the canopy corresponds to, (1) early morning hours in which the evening CO_2 build up is flushed into the atmosphere, and (2) late afternoon hours in which ground efflux and canopy respiration are large yet the atmospheric transport capacity is small.

The contrast between the important role of vegetation sources and sinks and the minor role of storage flux to the overall turbulent flux above the canopy is evident from the measurements as well. The mean measured F_s was two orders of magnitude smaller than the mean eddy-covariance flux at $z/z_h = 1.11$ for the seven day duration. Additionally, the overall comparison between modelled and measured mean CO_2 concentration and canopy fluxes did not significantly improve when the storage flux was included (see regression statistics in Table II).

4.5. DISCUSSION

Having demonstrated the ability of a modified *CANVEG* model to describe the canopy microclimate, such an approach can now be used to investigate how changes in physiological or biophysical properties alter biosphere-atmosphere water and carbon exchange. For example, changes or adjustments in foliage physiological properties or distribution due to elevated atmospheric CO_2 , as quantified from leaf, chamber, or Free Air CO_2 Enrichment (FACE) experiments, can be readily implemented in *CANVEG* to assess how much the net ecosystem carbon exchange and water vapour flux will be altered in response to such atmospheric CO_2 perturbations. Other immediate applications of the modified *CANVEG* approach includes guiding the development and assessment of simpler approaches, such as big-leaf approaches, which are currently used in many hydrologic, mesoscale, and climatic models.

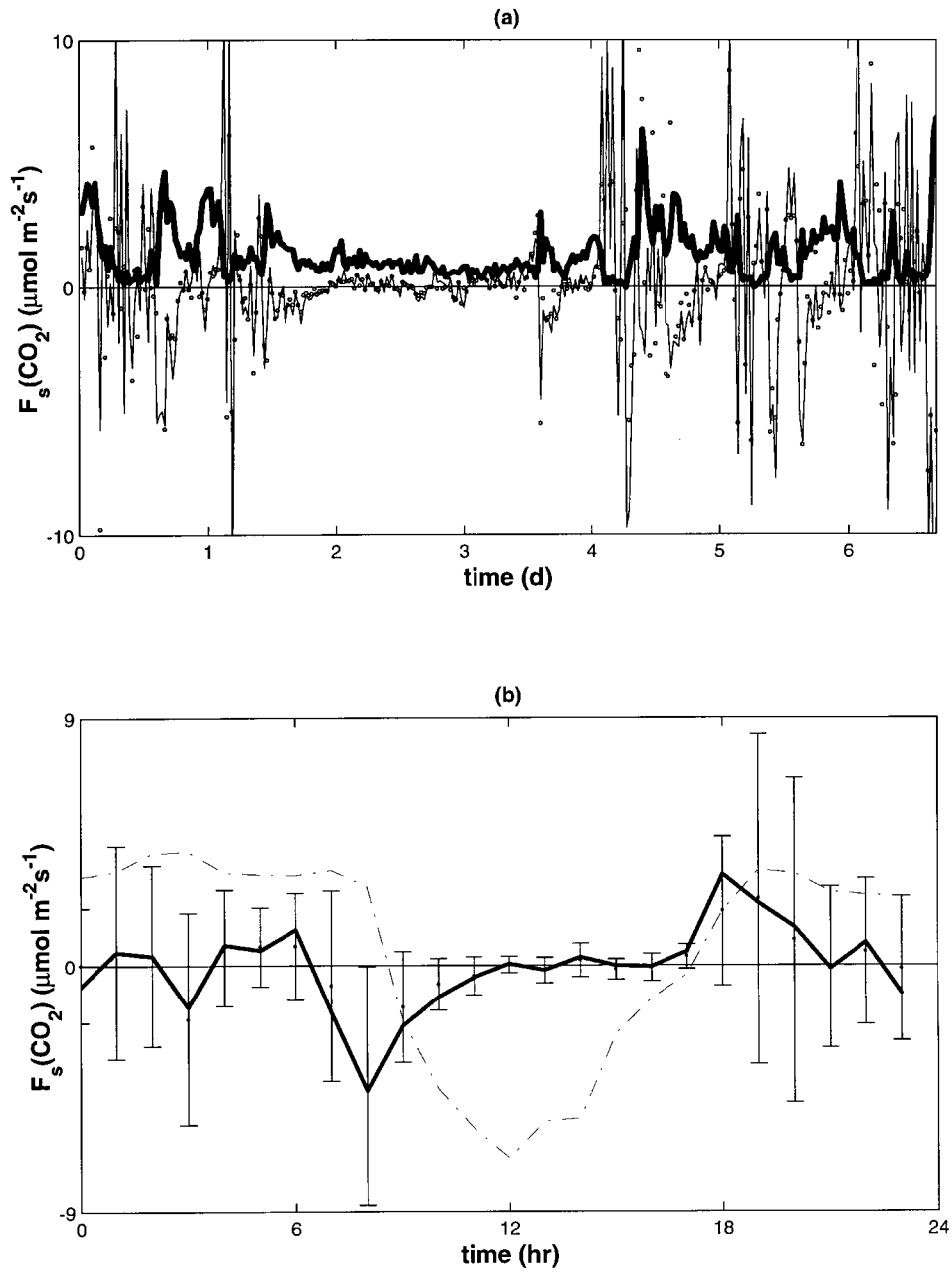


Figure 7. (a) Comparisons between measured (open circle) and modelled (solid line) depth-integrated CO₂ storage fluxes ($F_s(\text{CO}_2)$) on a 30-minute time step. The ground efflux is also shown (thick line); (b) Comparisons between ensemble measured (open circle) and modelled (solid line) depth-integrated CO₂ storage fluxes. The ensemble runs are constructed by averaging the modelled storage flux based on time of day. The modelled CO₂ flux at the canopy top is also shown (dashdot) for reference.

5. Conclusion

A one-dimensional canopy model that combines conservation of momentum (Eulerian), scalar mass (Lagrangian), radiative transfer, and physiological functions was developed and field-tested in a pine forest. This study demonstrated the following:

1. The σ_w profile computed with a second-order closure model is significantly different from their commonly assumed values in canopy Lagrangian transport models. This σ_w discrepancy translates to a significant difference (65%) in the dispersion matrix D_{ij} , particularly close to the ground surface.
2. The model underestimates leaf surface temperature by 2 °C, mainly because of poor parameterization of longwave reflectance for cloudy conditions.
3. The modelled source/sink profiles suggest that maximum CO₂ and water vapour source strengths are co-located with the maximum leaf area density. In contrast, maximum heat source strength is within the top 25% of the canopy. This source location difference is attributed, in part, to stomatal control on scalar, but not heat, transport. The broader implication of such findings is that the zero-plane displacement height, commonly computed from the centroid (or centre of pressure) of the source/sink distribution, is different for heat when compared to other scalars such as H₂O and CO₂.
4. The model reproduced well the measured time-depth concentration and integrated CO₂ storage flux within the canopy volume. The calculations also revealed that the magnitude of the CO₂ storage flux relative to the flux measured above the canopy is significant only during early morning and late afternoon hours. However, the overall contribution of storage flux, when depth and time averaged over the entire experiment duration, remains two orders of magnitude smaller than the fluxes at the canopy top.
5. The model reproduced well the eddy-covariance measured CO₂ and H₂O fluxes above the canopy despite the fact that, (1) the parameters of the g_s model were derived from leaf level measurements, and (2) the hydrologic conditions (i.e., $\bar{\theta} < 0.2$) were less than optimal for the application of the Collatz et al. (1991) physiological model. The proposed model performance for this forest was better than other *CANVEG* model results derived for well-watered homogeneous short vegetation such as soybeans (Baldocchi, 1992). The broader implication of the close agreement between modelled and measured fluxes is that the *CANVEG* model framework is useful for scaling up leaf-level physiological measurements to the ecosystem.

Acknowledgements

The authors would like to thank Greg Burkland, Andrew Palmiotti, and Galen Hon, for all their help during the experiment, and Keith Lewin and John Nagy for

their assistance in the CO₂/H₂O multi-port design and setup. This project was funded, in part, by the National Science Foundation (NSF-BIR 12333), and the U.S. Department of Energy (DOE) through the FACE-FACTS project and through the National Institute for Global Environmental Change (NIGEC) through the Southeast Regional Center at the University of Alabama, Tuscaloosa (DOE cooperative agreement DE-FC030-90ER61010).

Appendix A: Boundary Conditions and Parameterization of Random-Walk Modeling

The determination of D_{ij} is performed via the random-walk particle trajectory calculations of (3) and (4) and is given by

$$D_{ij} = \frac{c_i - c_R}{s_j \Delta z},$$

where c_i is the concentration at level index i generated by a unit source placed at level index j (not to be confused with intercellular concentration), and c_R is the reference concentration above the canopy. In the calculations of c_i , the canopy was divided into 14 layers, with 5000 fluid parcels released at each layer and allowed to disperse for at least 100 s (Baldocchi, 1992). The trajectory domain was restricted to seven times the canopy height. The time interval Δt was set to $0.05T_L$ as discussed in Hsieh et al. (1997). Raupach (1988) pointed out that the range of Δt is restricted and hence easy to select since in atmospheric turbulence flows, the acceleration time scale $T_k (\sim T_L R_e^{-1/2})$ is much less than the integral time scale. The boundary conditions for the particle trajectory are as follows:

1. *the bottom boundary*: fluid parcels intercepting the soil surface are perfectly reflected.
2. *the top boundary*: fluid parcels reaching the top of the domain are assumed to bounce back to conserve total mass.

We chose the particle trajectory domain to be sufficiently large ($= 7z_h$) so that inside and just above the canopy the concentration is not significantly influenced by this artificial top boundary.

Appendix B: The Wilson and Shaw (1977) Closure Model

Upon time and horizontally averaging the mean momentum and Reynolds stresses equations, and after performing the following simplifications:

1. steady-state adiabatic flow,
2. assuming the form-drag by the canopy can be modelled as a general drag force,
3. neglecting the viscous drag relative to the form drag,

4. closing all the triple-velocity products by a gradient – diffusion approximation (Donaldson, 1973; Mellor, 1973; Mellor and Yamada, 1974; Wilson and Shaw, 1977; Shaw, 1977; Wilson, 1988, 1989; Andren, 1990; Canuto et al., 1994; Abdella and McFarlane, 1997),
5. modeling the pressure-velocity gradients using return-to-isotropy principles,
6. assuming the viscous dissipation is isotropic and dependent on the local turbulence intensity (Mellor, 1973),
7. assuming horizontal homogeneity,

the second-order closure model of Wilson and Shaw (1977) reduces to:

Mean momentum:

$$0 = -\frac{d\langle\overline{u'w'}\rangle}{dz} - C_d a(z)\langle\bar{u}\rangle^2,$$

Shear stress:

$$0 = -\langle\overline{w'^2}\rangle\frac{d\langle\bar{u}\rangle}{dz} + 2\frac{d}{dz}\left(q\lambda_1\frac{d\langle\overline{u'w'}\rangle}{dz}\right) - \frac{q\langle\overline{u'w'}\rangle}{3\lambda_2} + C_w q^2\frac{d\langle\bar{u}\rangle}{dz},$$

Longitudinal variance:

$$0 = -2\langle\overline{u'w'}\rangle\frac{d\langle\bar{u}\rangle}{dz} + \frac{d}{dz}\left(q\lambda_1\frac{d\langle\overline{u'^2}\rangle}{dz}\right) + 2C_d a(z)\langle\bar{u}\rangle^3 \\ - \frac{q}{3\lambda_2}\left(\langle\overline{u'^2}\rangle - \frac{q^2}{3}\right) - \frac{2q^3}{3\lambda_3},$$

Lateral variance:

$$0 = \frac{d}{dz}\left(q\lambda_1\frac{d\langle\overline{v'^2}\rangle}{dz}\right) - \frac{q}{3\lambda_2}\left(\langle\overline{v'^2}\rangle - \frac{q^2}{3}\right) - \frac{2q^3}{3\lambda_3},$$

Vertical variance:

$$0 = \frac{d}{dz}\left(3q\lambda_1\frac{d\langle\overline{w'^2}\rangle}{dz}\right) - \frac{q}{3\lambda_2}\left(\langle\overline{w'^2}\rangle - \frac{q^2}{3}\right) - \frac{2q^3}{3\lambda_3},$$

with length scales defined by

$$\lambda_j = c_j L(z); \quad j = 1, 2, 3$$

$$L(z) = \max \left\{ \begin{array}{l} L(z - \Delta z) + \kappa \Delta z \\ \frac{\gamma}{C_d a(z)} \end{array} \right.$$

$$L(0) = 0.$$

Here, u_i ($u_1 = u, u_2 = v, u_3 = w$) are the instantaneous velocity components along x_i , x_i ($x_1 = x, x_2 = y, x_3 = z$) are the longitudinal, lateral, and vertical directions, respectively, $(\bar{\cdot})$ and $\langle \cdot \rangle$ denote time and horizontal averaging (Raupach and Shaw, 1982; Raupach et al., 1991), respectively, and primes denote departures from the temporal averaging operator, $q = \sqrt{\langle u'_i u'_i \rangle}$ is a characteristic turbulent velocity, λ_1, λ_2 , and λ_3 are characteristic length scales for the triple-velocity correlation, the pressure-velocity gradient correlation, and viscous dissipation, respectively, κ ($= 0.4$) is von Karman's constant, Δz is the depth increment defined by the discretization interval used to numerically solve the set of equations above and is different from the Δz_j defined in (2), C_d is the foliage drag coefficient, $a(z)$ is the leaf area density, γ is an empirical constant, and c_1, c_2, c_3 , and C_w are closure constants that can be determined such that the flow conditions well above the canopy reproduce established surface layer similarity relations. The numerical values of these constants are determined from measurements and similarity relations (see Katul and Albertson, 1998). With estimates of these five constants (c_1, c_2, c_3, C_w , and γ), the five ordinary differential equations listed above can be solved for the five flow variables $\langle \bar{u} \rangle, \langle \bar{u}'w' \rangle, \langle \bar{u}'^2 \rangle, \langle \bar{v}'^2 \rangle, \langle \bar{w}'^2 \rangle$ if appropriate boundary conditions are specified. The flow boundary conditions are assumed to approach the neutral atmospheric surface-layer similarity theory values (Panofsky and Dutton, 1984) well above the canopy, at $z/z_h \gg 1$,

$$\frac{d\langle \bar{u} \rangle}{dz} = \frac{u_*}{\kappa(z-d)},$$

$$\frac{\sigma_u}{u_*} = 2.4,$$

$$\frac{\sigma_v}{u_*} = 1.9,$$

$$\frac{\sigma_w}{u_*} = 1.25,$$

$$\frac{\langle \bar{u}'w' \rangle}{u_*^2} = -1.$$

At the ground surface, the boundary conditions are:

$$\langle \bar{u} \rangle = 0,$$

$$\frac{d\sigma_u}{dz} = 0,$$

$$\frac{d\sigma_v}{dz} = 0,$$

$$\frac{d\sigma_w}{dz} = 0,$$

$$\frac{d\langle \overline{u'w'} \rangle}{dz} = 0.$$

The numerical scheme to solve this set of equations is described in Katul and Albertson (1998, 1999). To demonstrate the differences among measured σ_w profile, Raupach's empirical σ_w profile and the σ_w profile generated by Wilson and Shaw's model described above, a multi-level experiment was carried out recently, and the experimental setup was detailed as follows.

The three velocity components and virtual potential temperature inside the canopy were measured at eight levels ($z = 1.3, 2.9, 4.8, 6.5, 8.5, 10.7, 12.1, 15.5$ m) between August 23 and August 30, 1999 with eight sets of CSAT3 sonic anemometers. Each CSAT3 was anchored on a horizontal bar extending 1.0 m from the walkup tower. The sampling frequency was 10 Hz for all sonic anemometers. All analog signals were digitized by a Campbell Scientific CR-9000 data logger, and transferred to a laptop computer for future processing. This experiment was performed at the Duke Forest AmeriFlux tower site where the turbulent flow properties, scalar fluxes, and scalar concentration profiles are acquired. The velocity statistics were collected over a wide range of atmospheric stability conditions. The comparisons among measured σ_w profile, Raupach's empirical σ_w profile, and the σ_w profile predicted using the second-order model are shown in Figure 8.

Appendix C: The Collatz et al. Model

Except for the stomatal conductance equation given in Section 2.3, all the equations needed for estimating leaf-scale CO_2 assimilation are given in this Appendix. Hence, for present purposes, \bar{C} represents mean CO_2 concentration (more formally, the 'mean' must represent time and horizontal averaging). Using the models of Farquhar et al. (1980) and Collatz et al. (1991), the net photosynthetic rate depends on light, CO_2 and leaf temperature and can be described as:

$$An \approx \min \left\{ \begin{array}{c} J_E \\ J_C \\ J_S \end{array} \right\} - R_d \quad (\text{C1})$$

where J_E , J_C and J_S are the assimilation rates restricted by light, ribulose biphosphate (R_uBP) carboxylase (or Rubisco), and the export rate of sucrose synthesis, respectively, and R_d is the respiration rate during day but in the absence of

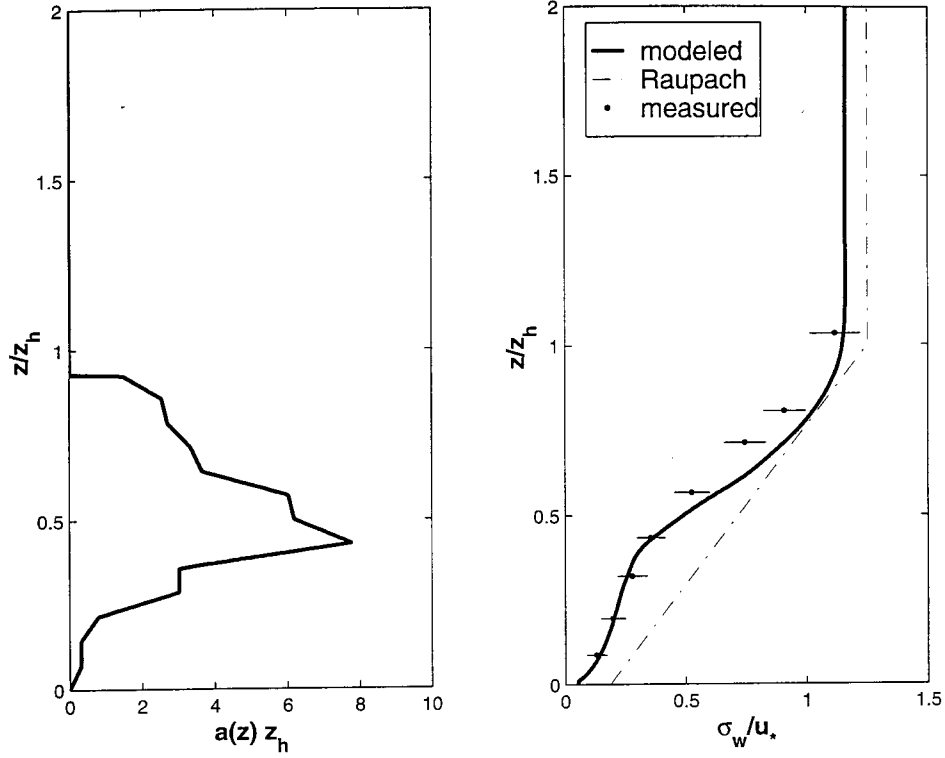


Figure 8. Comparisons between profiles of measured σ_w (dots), Raupach's (1988) empirical σ_w (dot-dash line), and the second-order closure model predicted σ_w (solid line). The normalized measured leaf area density is also shown.

photorespiration. Photorespiration is treated separately in the model parameterization. The gross assimilation rate ($= A_n + R_d$) is determined by the minimum of the three capacities since no photosynthesis can occur if the supply of any component is insufficient. In (C1), J_E describes the dependence of photosynthesis on light using:

$$J_E = \alpha_p e_m Q_p \frac{\bar{C} - \Gamma_*}{\bar{C}_i + 2\Gamma_*}, \quad (\text{C2})$$

where α_p is the leaf absorptivity for PAR, e_m is the maximum quantum efficiency for CO₂ uptake, Q_p is the PAR irradiance on the leaf, and the CO₂ compensation point, Γ_* , is the CO₂ concentration at which $A_n = 0$ in the absence of photorespiration, given by:

$$\Gamma_* = \frac{[\text{O}_2]}{2\omega}, \quad (\text{C3})$$

where $[\text{O}_2]$ is the oxygen concentration in air ($\approx 210 \text{ mmol mol}^{-1}$), and ω is a ratio of kinetic parameters describing the partitioning of R_uBP to the carboxylase or

oxygenase reactions of Rubisco. In other words, ω is a measure of the competition between CO_2 and O_2 for R_uBP that is intrinsic to the Rubisco enzyme in C_3 species.

J_C is the Rubisco-limited rate and is computed from:

$$J_C = \frac{V_m(\bar{C}_i - \Gamma_*)}{\bar{C}_i + K_c(1 + [\text{O}_2]/K_o)}, \quad (\text{C4})$$

where V_m is the maximum catalytic capacity of Rubisco per unit leaf area ($\mu\text{mol m}^{-2} \text{s}^{-1}$), K_c and K_o are the Michaelis constants for CO_2 fixation and O_2 inhibition with respect to CO_2 , respectively. Equation (C4) shows that J_C increases linearly with increasing \bar{C}_i , but approaches a maximum value at V_m under high CO_2 concentration conditions that are generally not encountered under current conditions.

J_S is the capacity for the export or utilization of photosynthesis products, and sucrose synthesis is most likely the rate limiting step (see Collatz et al., 1991). J_S is estimated by:

$$J_S = V_m/2. \quad (\text{C5})$$

The rapid cutoff transition implied in (C1) suggests that to be more realistic, a mathematical scheme needs to be applied to account for the gradual transition from one limitation to another, and to allow for some co-limitation among J_E , J_C and J_S . We used the quadratic functions described in Collatz et al. (1991) to circumvent these limitations (not shown here).

We assume that the respiration rate R_d in (C1) is linearly related to V_m by (Farquhar et al. (1980))

$$R_d = 0.015V_m. \quad (\text{C6})$$

The parameterization of model kinetic variables in terms of temperature dependence follows the procedure of Campbell and Norman (1998), in which five parameters are adjusted for temperature: K_c , K_o , ω , V_m and R_d . For the first three parameters, a modified Q_{10} temperature function is employed:

$$k = k_{25} \exp[y(T_s - 25)], \quad (\text{C7})$$

where k is defined at leaf surface temperature T_s , k_{25} is the value of the parameter at 25°C , and y is the temperature coefficient for that parameter from Campbell and Norman (1998). In addition, V_m and R_d are adjusted by a more complex function incorporating deactivation effects at extreme high temperatures:

$$V_m = \frac{V_{m,25} \exp[0.088(T_s - 25)]}{1 + \exp[0.29(T_s - 41)]} \quad (\text{C8})$$

and

$$R_d = \frac{R_{d,25} \exp[0.069(T_s - 25)]}{1 + \exp[1.3(T_s - 55)]}, \quad (\text{C9})$$

where $V_{m,25}$ and $R_{d,25}$ are the values of V_m and R_d at 25 °C, respectively. This equation assumes that these two quantities are significantly reduced when $T_s > 41$ °C for V_m and $T_s > 55$ °C for R_d .

Finally, \bar{C}_s , \bar{C}_i , and \bar{C}_a are related by:

$$\bar{C}_i = \bar{C}_s - \frac{A_n}{g_s} \quad (\text{C10})$$

and

$$\bar{C}_s = \bar{C}_a - \frac{A_n}{g_b}, \quad (\text{C11})$$

where $g_s (= r_s^{-1})$ is the stomatal conductance and $g_b (= r_b^{-1})$ is the leaf boundary layer conductance.

References

- Abdella, K. and McFarlane, N.: 1997, 'A New Second-Order Turbulence Closure Scheme for the Planetary Boundary Layer', *J. Atmos. Sci.* **54**, 1850–1867.
- Andren, A.: 1990, 'Evaluation of a Turbulence Closure Scheme Suitable for Air Pollution Applications', *J. Appl. Meteorol.* **29**, 224–239.
- Aphalo, P. J. and Jarvis, P. G.: 1991, 'Do Stomata Respond to Relative Humidity?', *Plant Cell Environ.* **14**, 127–132.
- Baldocchi, D. D.: 1992, 'A Lagrangian Random-Walk Model for Simulating Water Vapour, CO₂ and Sensible Heat Flux Densities and Scalar Profiles over and within a Soybean Canopy', *Boundary-Layer Meteorol.* **61**, 113–144.
- Baldocchi, D. D.: 1997, 'Flux Footprints within and over Forest Canopies', *Boundary-Layer Meteorol.* **85**, 273–292.
- Baldocchi, D. D. and Meyers, T.: 1998, 'On Using Eco-Physiological, Micrometeorological and Biogeochemical Theory to Evaluate Carbon Dioxide, Water Vapour and Trace Gas Fluxes over Vegetation: A Perspective', *Agric. For. Meteorol.* **90**, 1–25.
- Baldocchi, D. D., Vogel, C. A., and Hall, B.: 1997, 'Seasonal Variation of Carbon Dioxide Exchange Rates above and below a Boreal Jack Pine Forest', *Agric. For. Meteorol.* **83**, 147–170.
- Campbell, G. S. and Norman, J. M.: 1998, *An Introduction to Environmental Biophysics*, Springer-Verlag, New York, pp. 148–259.
- Canuto, V. M., Minotti, F., Ronchi, C., Ypma, R. M., and Zeman, O.: 1994, 'Second-Order Closure PBL Model with New Third-Order Moments: Comparison with LES Data', *J. Atmos. Sci.* **51**, 1605–1618.
- Collatz, G. J., Ball, J. T., Grivet, C., and Berry, J. A.: 1991, 'Physiological and Environmental Regulation of Stomatal Conductance, Photosynthesis and Transpiration: A Model that Includes a Laminar Boundary Layer', *Agric. For. Meteorol.* **54**, 107–136.

- Corrsin, S.: 1974, 'Limitations of Gradient Transport Models in Random Walks and in Turbulence', *Adv. Geophys.* **18A**, 25–60.
- Deardorff, J. W.: 1978, 'Closure of Second and Third Moment Rate Equations for Diffusion in Homogeneous Turbulence', *Phys. Fluids* **21**, 525–530.
- De Pury, D. G. G. and Farquhar, G. D.: 1997, 'Simple Scaling of Photosynthesis from Leaves to Canopies without the Errors of Big-Leaf Models', *Plant Cell Environ.* **20**, 537–557.
- Donaldson, C. and Du P.: 1973, 'Construction of a Dynamic Model for the Production of Atmospheric Turbulence and the Dispersion of Atmospheric Pollutants', in *Workshop on Micrometeorology*, *Amer. Meteorol. Soc.* pp. 313–392.
- Ellsworth, D. S.: 1999, 'CO₂ Enrichment in a Maturing Pine Forest: Are CO₂ Exchange and Water Status in the Canopy Affected?', *Plant Cell Environ.* **22**, 461–472.
- Ewers, B. E. and Oren, R.: 2000, 'Analyses of Assumptions and Errors in the Calculation of Stomatal Conductance from Sap Flux Measurements', *Tree Physiol.* **20**, in press.
- Fan, S.-M., Goulden, M. L., Munger, J. W., Daube, B. C., Bakwin, P. S., Wofsy, S. C., Amthor, J. S., Fitzjarrald, D. R., Moore, K. E., and Moore, T. R.: 1995, 'Environmental Controls on the Photosynthesis and Respiration of a Boreal Lichen Woodland: A Growing Season of Whole-Ecosystem Exchange Measurements by Eddy Correlation', *Oecologia* **102**, 443–452.
- Farquhar, G. D., Caemmerer, S. von, and Berry, J. A.: 1980, 'A Biochemical Model of Photosynthetic CO₂ Assimilation in Leaves of C₃ Species', *Planta* **149**, 78–90.
- Grace, J., Lloyd, J. McIntyre, J., Miranda, A., Meir, P., Miranda, H., Moncrieff, J., Massheder, J., Wright, I., and Gash, J.: 1995, 'Fluxes of Carbon Dioxide and Water Vapour over an Undisturbed Tropical Forest in South-West Amazonia', *Global Change Biol.* **1**, 1–12.
- Harley, P. C., Thomas, R. B., Reynolds, J. F., and Strain, B. R.: 1992, 'Modeling Photosynthesis of Cotton Grown in Elevated CO₂', *Plant Cell Environ.* **15**, 271–282.
- Harley, P. C., Weber, J. A., and Gates, D. M.: 1985, 'Interactive Effects of Light, Leaf Temperature, CO₂ and O₂ on Photosynthesis in Soybean', *Planta* **165**, 249–263.
- Hollinger, D. Y., Kelliher, F. M., Byers, J. N., Hunt, J. E., McSeveny, T. M., and Weir, P. L.: 1994, 'Carbon Dioxide Exchange between an Undisturbed Old-Growth Temperate Forest and the Atmosphere', *Ecology* **75**, 134–150.
- Hsieh, C. I., Katul, G. G., Schieldge, J., Sigmon, J. T., and Knoerr, K. K.: 1997, 'The Lagrangian Stochastic Model for Fetch and Latent Heat Flux Estimation above Uniform and Nonuniform Terrain', *Water Resour. Res.* **33**, 427–438.
- Kaimal, J. C. and Finnigan, J. J.: 1994, *Atmospheric Boundary Layer Flows: Their Structure and Measurements*, Oxford Press, 289 pp.
- Katul, G. G. and Albertson, J. D.: 1998, 'An Investigation of Higher Order Closure Models for a Forested Canopy', *Boundary-Layer Meteorol.* **89**, 47–74.
- Katul, G. G. and Albertson, J. D.: 1999, 'Modeling CO₂ Sources, Sinks, and Fluxes within a Forest Canopy', *J. Geophys. Res.* **104**, 6081–6091.
- Katul, G. G. and Chang, W.-H.: 1999, 'Principal Length Scales in Second-Order Closure Models for Canopy Turbulence', *J. Appl. Meteorol.* **38**, 1631–1643.
- Katul, G. G., Hsieh, C. I., Bowling, D., Clark, K., Shurpali, N., Turnipseed, A., Albertson, J., Tu, K., Hollinger, D., Evans, R., Offerle, B., Anderson, D., Ellsworth, D., Vogel, C., and Oren, R.: 1999, 'Spatial Variability of Turbulent Fluxes in the Roughness Sublayer of an Even-Aged Pine Forest', *Boundary-Layer Meteorol.* **93**, 1–28.
- Katul, G. G., Oren, R., Ellsworth, D., Hsieh, C. I., Phillips, N., and Lewin, K.: 1997a, 'A Lagrangian Dispersion Model for Predicting CO₂ Sources, Sinks, and Fluxes in a Uniform Loblolly Pine (*Pinus taeda* L.) Stand', *J. Geophys. Res.* **102**, 9309–9321.
- Katul, G. G., Hsieh, C. I., Kuhn, G., Ellsworth, D., and Nie, D.: 1997b, 'The Turbulent Eddy Motion at the Forest-Atmosphere Interface', *J. Geophys. Res.* **102**, 13409–13421.
- Lee, X.: 1998, 'On Micrometeorological Observations of Surface-Air Exchange over Tall Vegetation', *Agric. For. Meteorol.* **91**, 39–49.

- Leuning, R.: 1995, 'A Critical Appraisal of a Combined Stomatal-Photosynthesis Model for C₃ Plants', *Plant Cell Environ.* **18**, 339–357.
- Lewellen, W. S., Teske, M. E., and Sheng, Y. P.: 1980, 'Micrometeorological Applications of a Second-Order Closure Model of Turbulent Transport', in L. J. S. Bradbury, F. Durst, B. E. Launder, F. W. Schmidt, and J. H. Whitelaw (eds.), *Turbulent Shear Flows II*, Springer-Verlag, pp. 366–378.
- Luhar, A. K. and Britter, R. E.: 1989, 'A Random Walk Model for Dispersion in Inhomogeneous Turbulence in a Convective Boundary Layer', *Atmos. Environ.* **23**, 1911–1924.
- Massman, W. J. and Weil, J. C.: 1999, 'An Analytical One-Dimensional Second-Order Closure Model of Turbulence Statistics and the Lagrangian Time Scale within and above Plant Canopies of Arbitrary Structure', *Boundary-Layer Meteorol.* **91**, 81–107.
- Mellor, G.: 1973, 'Analytic Prediction of the Properties of Stratified Planetary Boundary Layer', *J. Atmos. Sci.* **30**, 1061–1069.
- Mellor, G. L. and Yamada, T.: 1974, 'A Hierarchy of Turbulence Closure Models for Planetary Boundary Layers', *J. Atmos. Sci.* **31**, 1791–1806.
- Meyers, T. P. and Baldocchi, D. D.: 1991, 'The Budgets of Turbulent Kinetic Energy and Reynolds Stress within and above a Deciduous Forest', *Agric. For. Meteorol.* **53**, 207–222.
- Meyers, T. P. and Paw U, K. T.: 1986, 'Testing of a Higher-Order Closure Model for Modeling Airflow within and above Plant Canopies', *Boundary-Layer Meteorol.* **37**, 297–311.
- Meyers, T. P. and Paw U, K. T.: 1987, 'Modeling the Plant Canopy Micrometeorology with Higher-Order Closure Principles', *Agric. For. Meteorol.* **41**, 143–163.
- Monteith, J. L.: 1995, 'Accommodation between Transpiring Vegetation and the Convective Boundary Layer', *J. Hydrol.* **166**, 251–263.
- Mott, K. A. and Parkhurst, D. F.: 1991, 'Stomatal Responses to Humidity in Air and Helox', *Plant Cell Environ.* **14**, 509–515.
- Oren, R., Ewers, B., Todd, P., Phillips, N., and Katul, G. G.: 1998, 'Water Balance Delineates the Soil Layer in which Moisture Affects Canopy Conductance', *Ecol. Applications* **8**, 990–1002.
- Panofsky, H. A. and Dutton, J. A.: 1984, *Atmospheric Turbulence: Models and Methods for Engineering Applications*, Wiley-Interscience, New York, 397 pp.
- Pataki, D. E., Oren, R., Katul, G. G., and Sigmon, J.: 1998, 'Canopy Conductance of *Pinus Taeda*, *Liquidambar styraciflua*, and *Quercus Phellos* under Varying Atmospheric and Soil Water Conditions', *Tree Physiol.* **18**, 307–315.
- Penman, H. L.: 1948, 'Natural Evaporation from Open Water, Bare Soil and Grass', *Proc. Roy. Soc. London, Ser. A.* **193**, 120–146.
- Raupach, M. R.: 1988, 'Canopy Transport Processes', in W. L. Steffen and O. T. Denmead (eds.), *Flow and Transport in the Natural Environment*, Springer-Verlag, Berlin, pp. 95–127.
- Raupach, M. R.: 1989a, 'A Practical Lagrangian Method for Relating Scalar Concentrations to Source Distributions in Vegetation Canopies', *Quart. J. Roy. Meteorol. Soc.* **115**, 609–632.
- Raupach, M. R.: 1989b, 'Applying Lagrangian Fluid Mechanics to Infer Scalar Source Distributions from Concentration Profiles in Plant Canopies', *Agric. For. Meteorol.* **47**, 85–108.
- Raupach, M. R. and Shaw, R. H.: 1982, 'Averaging Procedures for Flow within Vegetation Canopies', *Boundary-Layer Meteorol.* **22**, 79–90.
- Raupach, M. R., Antonia, R. A., and Rajagopalan, S.: 1991, 'Rough-Wall Turbulent Boundary Layers', *Appl. Mech. Rev.* **44**, 1–25.
- Sawford, B. L.: 1985, 'Lagrangian Statistical Simulation of Concentration Mean and Fluctuation Fields', *J. Clim. Appl. Meteorol.* **24**, 1152–1166.
- Sawford, B. L.: 1993, 'Recent Developments in the Lagrangian Stochastic Theory of Turbulent Dispersion', *Boundary-Layer Meteorol.* **62**, 197–215.
- Schuepp, P. H.: 1993, 'Tansley Review No. 59: Leaf Boundary Layers', *New Phytologist* **125**, 477–507.

- Shaw, R. H.: 1977, 'Secondary Wind Speed Maxima inside Plant Canopies', *J. Appl. Meteorol.* **16**, 514–521.
- Shaw, R. H. and Pereira, A. R.: 1982, 'Aerodynamic Roughness of a Plant Canopy: A Numerical Experiment', *Agric. Meteorol.* **26**, 51–65.
- Sreenivasan, K. R., Tavoularis, S., and Corrsin, S.: 1982, 'A Test of Gradient Transport and its Generalization', *Turbulent Shear Flow III*, Springer-Verlag, New York, pp. 96–112.
- Thomson, D. J.: 1987, 'Criteria for the Selection of Stochastic Models of Particle Trajectories in Turbulent Flows', *J. Fluid Mech.* **180**, 529–556.
- Wilson, J. D.: 1988, 'A Second Order Closure Model for Flow through Vegetation', *Boundary-Layer Meteorol.* **42**, 371–392.
- Wilson, J. D.: 1989, 'Turbulent Transport within the Plant Canopy', in *Estimation of Areal Evapotranspiration*, Vol. 177, IAHS Publ., pp. 43–80.
- Wilson, J. D. and Sawford, B. L.: 1996, 'Review of Lagrangian Stochastic Models for Trajectories in the Turbulent Atmosphere', *Boundary-Layer Meteorol.* **78**, 191–210.
- Wilson, N. R. and Shaw, R. H.: 1977, 'A Higher Order Closure Model for Canopy Flow', *J. Appl. Meteorol.* **16**, 1198–1205.
- Wofsy, S. C., Goulden M. L., Munger, J. W., Fan, S.-M., Bakwin, P. S., Daube, B. C., Bassow, S. L., and Bazzaz, F. A.: 1993, 'Net Exchange of CO₂ in a Mid-Latitude Forest', *Science* **260**, 1314–1317.